

Feature Article

## Excitonic Solar Cells

Brian A. Gregg

*J. Phys. Chem. B*, **2003**, 107 (20), 4688-4698 • DOI: 10.1021/jp022507x

Downloaded from <http://pubs.acs.org> on December 4, 2008

### More About This Article

---

Additional resources and features associated with this article are available within the HTML version:

- Supporting Information
- Links to the 73 articles that cite this article, as of the time of this article download
- Access to high resolution figures
- Links to articles and content related to this article
- Copyright permission to reproduce figures and/or text from this article

[View the Full Text HTML](#)



ACS Publications  
High quality. High impact.

## FEATURE ARTICLE

## Excitonic Solar Cells

Brian A. Gregg

National Renewable Energy Laboratory, 1617 Cole Boulevard, Golden, Colorado 80401-3393

Received: December 3, 2002; In Final Form: March 3, 2003

Existing types of solar cells may be divided into two distinct classes: conventional solar cells, such as silicon p–n junctions, and excitonic solar cells, XSCs. Most organic-based solar cells, including dye-sensitized solar cells, DSSCs, fall into the category of XSCs. In these cells, excitons are generated upon light absorption, and if not created directly at the heterointerface as in DSSCs, they must diffuse to it in order to photogenerate charge carriers. The distinguishing characteristic of XSCs is that charge carriers are generated and *simultaneously* separated across a heterointerface. In contrast, photogeneration of free electron–hole pairs occurs throughout the bulk semiconductor in conventional cells, and carrier separation upon their arrival at the junction is a subsequent process. This apparently minor mechanistic distinction results in fundamental differences in photovoltaic behavior. For example, the open circuit photovoltage  $V_{oc}$  in conventional cells is limited to less than the magnitude of the band bending  $\Phi_{bi}$ ; however,  $V_{oc}$  in XSCs is commonly greater than  $\Phi_{bi}$ . Early work on solid-state excitonic solar cells is described as are excitonic processes in general and the use of carrier-selective (energy-selective) contacts to enhance  $V_{oc}$ . Then studies of DSSCs, which provide a particularly simple example of XSCs, are described. A general theoretical description applicable to all solar cells is employed to quantify the differences between conventional and excitonic cells. The key difference is the dominant importance, in XSCs, of the photoinduced chemical potential energy gradient  $\nabla\mu_{hv}$ , which was created by the interfacial exciton dissociation process. Numerical simulations demonstrate the difference in photoconversion mechanism caused solely by changing the spatial distribution of the photogenerated carriers. Finally, the similarities and differences are explored between the three major types of XSCs: organic semiconductor cells with planar interfaces, bulk heterojunction cells, and DSSCs.

## I. Introduction

Conventional solar cells, epitomized by the silicon p–n junction cell, were invented in the 1950s and first commercialized in the 1960s for use in the space program.<sup>1</sup> Since then, there have been rapid advances in the efficiency and reliability of these cells, along with substantial decreases in cost. The nascent photovoltaic industry has been growing rapidly as a result of these advances. Nevertheless, the price of solar power is still greater than the price of power from the electrical grid in industrialized nations, partly because the costs of the pollution generated by conventional power sources are not included in their prices.

There is an increasing amount of research devoted to potentially less expensive types of solar cells such as those based on organic dyes and pigments;<sup>2–5</sup> these have been studied since the late 1950s,<sup>6–8</sup> albeit at a fairly low level until recently. One of the great promises of organic electronics is that, once the physical requirements for a certain application are clearly understood, synthetic chemists can produce compounds having these characteristics. For the moment, however, the primary challenge is still to understand the physical requirements. A fundamental difference between organic solar cells and conventional solar cells was recognized almost immediately: light absorption results in the formation of excitons in organic materials rather than the free electron–hole pairs directly

produced in inorganic semiconductors, such as silicon.<sup>8–10</sup> An exciton in an organic semiconductor (usually a Frenkel exciton)<sup>11</sup> is sometimes considered to be a bound electron–hole pair. However, because of its electroneutrality and the strong binding between the electron and the hole, it is often better characterized as a mobile excited state.<sup>12</sup> Although the distinction between the photogeneration of excitons in organic semiconductors and of free electron–hole pairs in inorganic semiconductors was made early on, the consequences of this distinction are just beginning to be fully appreciated.<sup>12–15</sup> This paper examines the fundamental changes in photoconversion mechanism caused by this difference. With minimal oversimplification, I believe it is possible to separate existing solar cells into two distinct categories on the basis of their charge-generation mechanisms: conventional solar cells and excitonic solar cells. The latter category, XSCs, consists of cells in which light absorption results in the production of a transiently localized excited state that cannot thermally dissociate (binding energy  $\gg kT$ ) in the chemical phase in which it was formed. Examples of XSCs include molecular semiconductor solar cells,<sup>16–19</sup> conducting polymer solar cells,<sup>2,3,20–27</sup> dye-sensitized solar cells (DSSCs),<sup>4,5,15,28–31</sup> and probably also the proposed, but not yet realized, quantum dot solar cells.<sup>32</sup> In all these cases, charge generation via interfacial exciton dissociation results in

a photoconversion mechanism that is fundamentally different from that in conventional solar cells.

Section II of this paper describes some of the early work on excitonic processes in organic semiconductors and solar cells. When electrically symmetrical cells designed to measure the photoconductivity of some new organic semiconductors produced instead a stable and reproducible photovoltaic effect, it became clear that organic materials could generate a photovoltaic effect by mechanisms that are not available to conventional inorganic semiconductors.<sup>13</sup> Section III further characterizes the asymmetric interfacial exciton dissociation process and shows that it can overwhelm the influence of an internal electric field, driving photocurrent in the opposite direction from that expected by the “conventional” mechanism. The strength of this effect can be enhanced through the use of carrier-selective (i.e., potential energy-selective) contacts that permit exciton dissociation to occur only in one polarity. The formation, transport, and dissociation of excitons are described in section IV. Section V provides a brief description of dye-sensitized solar cells—in some respects the simplest of the XSCs. The sometimes-overlooked force derived from the interfacial excited state dissociation process is most clearly evident in DSSCs because complicating processes, such as exciton transport, play no role, and because the competing force of the internal electric field is practically eliminated by the electrolyte solution that permeates the nanoporous device. A conceptual and theoretical description of photoconversion processes that is appropriate for both conventional and excitonic solar cells is developed in section VI. It quantifies the essential difference between the two classes of cells and delineates the complementary roles of the two fundamental forces in solar cells: the gradients of the electrical and chemical potential energies  $\nabla U$  and  $\nabla \mu$ , respectively. The numerical simulations of section VII demonstrate the major differences in photovoltaic (PV) behavior for two cell types that differ *only* in the spatial location of the photogenerated charge carriers. Finally, the relationships between the three existing types of XSCs—organic semiconductor cells with planar interfaces, bulk heterojunction cells, and DSSCs—are discussed in section VIII. Their differences show the breadth of behavior encompassed by the XSC concept, while their similarities highlight the fundamental distinctions between XSCs and conventional PV cells.

## II. Recognizing the Significance of the Interfacial Exciton Dissociation Process

The mechanism by which silicon p–n junction solar cells function is so well-known<sup>1,33</sup> that it is sometimes mistaken for the only possible photoconversion mechanism. One of its distinguishing features is that the open circuit photovoltage  $V_{oc}$  cannot exceed the magnitude of the “built-in” electrical potential energy difference across the cell at equilibrium,  $\phi_{bi}$ , also known as the “band bending”.<sup>17,33,34</sup> Natural photosynthesis,<sup>35–37</sup> however, does not employ a p–n junction nor is the free energy stored in its intermediates and products limited to some internal electrical potential difference. Realistically, therefore, we should not expect solar cells made from organic semiconductors (some of which are similar to the molecules employed in photosynthesis) to necessarily function by the same mechanism as silicon p–n junctions. Nevertheless, this is often assumed, albeit with a mechanism modified by the exciton formation, diffusion, and dissociation processes.

In early studies, excitons were often assumed to dissociate in the electric field at the organic “p–n junction”. This mechanism would then lead to behavior similar to that of an

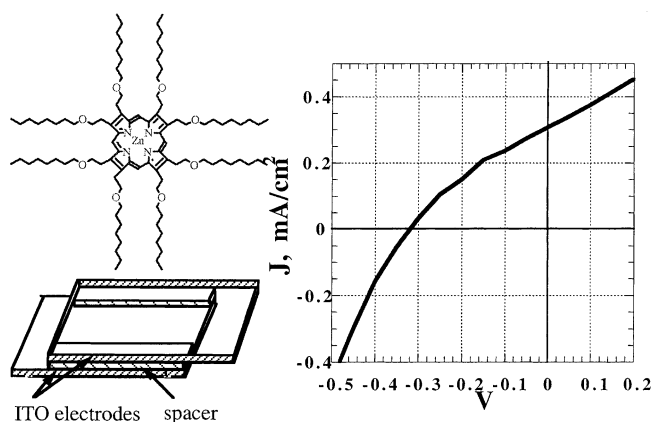


**Figure 1.** The current density–voltage,  $J$ – $V$ , curve (right) of a 2.5  $\mu\text{m}$  thick symmetrical (ITO/Porphyrin/ITO) cell (shown at bottom left) containing a capillary-filled liquid crystal porphyrin, ZnOOEP, (top left) under  $\sim 1$  sun illumination. Turning the cell around and illuminating through the other electrode gave identical results. (Data from ref 13.)

inorganic semiconductor p–n junction, namely, that  $qV_{oc} < \phi_{bi}$  (where  $q$  is the electronic charge), because the junction field would be necessary to *generate* charge carriers via exciton dissociation. Recent studies, however, show that the whole notion of an organic p–n junction is problematic, partly because of the high diffusion coefficients of the “dopants”, and that a true organic p–n junction may not yet have been realized.<sup>38–41</sup> Furthermore, excitons in the average organic semiconductor are so strongly bound that they are practically unaffected by internal electric fields.<sup>12,42–44</sup>

The first photovoltaic effect in an organic crystal sandwiched between two identical electrodes was reported by Kallman and Pope in 1959.<sup>6</sup> They used 5  $\mu\text{m}$  thick single crystals of anthracene to separate two solutions of NaCl. Upon illumination, a photovoltage of 200 mV was generated between the two solutions, the illuminated side charging negative. They were not able to propose a detailed mechanism to account for the photovoltage but concluded that charge transfer across the illuminated interface must occur by a different mechanism than charge transfer across the dark interface. Seven years later, Geacintov, Pope, and Kallman reported studies of single-crystal tetracene sandwiched between two chambers of distilled water.<sup>45</sup> They again observed a PV effect and concluded that the majority of the photocurrent was caused by exciton diffusion to the illuminated tetracene/water interface followed by electron injection into the water. A small percentage of the photocurrent originated from photogeneration of carriers in the bulk tetracene (photoconductivity). Unfortunately, these pioneering studies went almost unnoticed.

Two decades later we wished to study the photoconductivity of our newly synthesized liquid crystal (LC) porphyrins, such as zinc octakis(octyloxyethyl)porphyrin, ZnOOEP (structure shown in Figure 1).<sup>46</sup> We prepared electrically symmetrical cells consisting of two ITO (indium–tin oxide) electrodes separated by 2–5  $\mu\text{m}$  spacers. ZnOOEP in its isotropic liquid phase was capillary-filled between the electrodes and then cooled through the LC phase into the solid state at room temperature. This resulted in a highly oriented, polycrystalline film of LC porphyrin. Since the empty cell was symmetrical, and it was filled with an isotropic liquid, the final device could not contain a macroscopic internal electric field ( $\phi_{bi} = 0$ ). Nevertheless, illumination resulted in a stable and reproducible photovoltaic effect.<sup>13</sup> The PV effect was surprisingly strong (Figure 1) considering the 2–5  $\mu\text{m}$  thickness of the organic film: for example,  $V_{oc} = 330$  mV and  $J_{sc} = 0.3$  mA/cm<sup>2</sup> at approximately

1 sun illumination intensity ( $75 \text{ mW/cm}^2$ ). The illuminated electrode always charged negative; if the cell was turned around, the newly illuminated electrode (which was positive as the dark electrode) would charge negative in less than a minute. Cells could be illuminated for weeks, passing thousands of electrons per porphyrin, without any change. It was obvious that this behavior could not be explained by the conventional model of solar cells<sup>13</sup> nor was it caused by a Dember effect.<sup>13,47</sup>

We explained these results by a kinetic model. There were two *photoproduced* asymmetries in these cells which were, in the dark, completely symmetrical: (1) Light was incident on only one side of these optically thick cells, thus producing excitons primarily near this electrode (if both electrodes were illuminated simultaneously, the PV effect disappeared and only photoconductivity was observed). (2) We assumed that the exciton dissociation process at the porphyrin/ITO interface was kinetically asymmetric: that is, exciton dissociation by electron injection into the ITO electrode, leaving a hole behind in the porphyrin, was kinetically more facile than the opposite dissociation process of hole injection into the ITO. No further assumptions were necessary to explain the results: the simple fact that electrons were preferentially injected into the illuminated ITO electrode, and holes into the porphyrin, necessarily resulted in a photovoltaic effect. We were aware, of course, that the photoseparation of charge carriers in a cell that initially contained no electric field would generate an electric field due to the Coulomb attraction between the carriers. This photogenerated electric field would oppose further charge separation. Therefore, the measured  $V_{oc}$  ( $0.25\text{--}0.35 \text{ V}$ ) indicated the strength of this asymmetric interfacial exciton dissociation process: it just sufficed to drive charge carriers up an opposing electric potential difference equal to  $V_{oc}$ . As in the work of Geacintov et al.,<sup>45</sup> it was clear from photocurrent action spectra measurements that a small fraction of the absorbed photons directly generated carriers in the bulk. Thus, the PV effect, although driven by asymmetric interfacial exciton dissociation, was modified by the photoconductivity resulting from the bulk generation of carriers, presumably at trap sites.<sup>13</sup>

A year later, the nanoporous dye-sensitized solar cell, DSSC, developed by Grätzel and co-workers, was announced.<sup>5</sup> It achieved an efficiency ( $\sim 7\%$ ) far higher than other nonconventional solar cells and immediately attracted great interest. The correct theoretical description of DSSCs was not apparent at the time, but is now becoming well accepted.<sup>4,15,48,49</sup> There were some similarities between DSSCs and our solid-state LC porphyrin cells: both appeared to be driven by the interfacial dissociation of excited states which resulted in the generation of electrons in one chemical phase and holes in the other. But there were also substantial differences that at first obscured the similarities.

### III. Carrier-Selective Contacts and the Interfacial Exciton Dissociation Process

Having proposed a mechanism to explain the photovoltaic effect in symmetrical organic PV cells, we tested some of its predictions. It was the kinetic asymmetry of the interfacial exciton dissociation process that gave rise to the PV effect in our model. That is, all else being equal, the more rapidly electrons were injected across the interface relative to holes (or vice versa) the greater the photovoltage should be. In our original configuration (Figure 1), excitons could dissociate by either electron injection or hole injection into the illuminated ITO electrode; electron injection was simply faster. Therefore, we sought carrier-selective contacts that would more completely

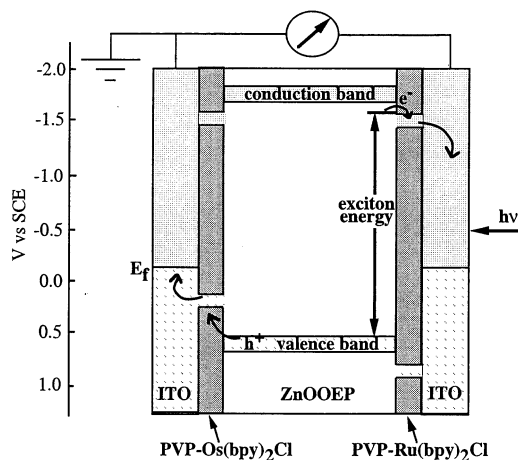


**Figure 2.** The use of carrier-selective contacts to improve the photovoltage. If the exciton energy and bandedge potentials are known, contacts can be devised that will pass primarily electrons or primarily holes. The lower two gaps drawn in the redox polymer films indicate the film oxidation potentials; the upper ones indicate their reduction potentials. In this case, the use of selective contacts increased  $V_{oc}$  from  $0.3$  to  $1.0 \text{ V}$ , without any band bending in the equilibrium cell. SCE = standard calomel electrode.

rectify the exciton dissociation process. (Such carrier-selective, or energy-selective, contacts were recently proposed to be a necessary requirement for realizing high-efficiency “hot-carrier” solar cells.<sup>32,50,51</sup>) We first experimented with thin films of redox polymers on ITO electrodes.<sup>52</sup> Given the excited-state potentials of our LC porphyrin and the redox potentials of the polymers, we reasoned that a thin film of poly(vinylpyridine) complexed to Ru(II)-bis(bipyridine)-Cl ( $\text{PVP-Ru(bpy)}_2\text{Cl}$ )<sup>53</sup> covering the illuminated ITO electrode should function as an electron-selective contact (Figure 2). Excitons could not dissociate via hole injection into the electrode because excited ZnOOEP cannot oxidize  $\text{PVP-Ru(bpy)}_2\text{Cl}$  (Figure 2). Experimentally, this film increased  $V_{oc}$  to  $\sim 0.6 \text{ V}$  compared to  $\sim 0.3 \text{ V}$  without the carrier-selective contact. Likewise, we reasoned that a thin film of poly(vinylpyridine) complexed to Os(II)-bis(bipyridine)-Cl ( $\text{PVP-Os(bpy)}_2\text{Cl}$ )<sup>53,54</sup> should function as a moderately selective contact for holes, although it could also pass some electrons (Figure 2). This film on the illuminated electrode inverted  $V_{oc}$  to  $\sim -0.1 \text{ V}$ . Both of these polymers were electrically neutral as deposited and impedance measurements over the frequency range  $10 \text{ mHz} - 1 \text{ kHz}$  showed no measurable band bending in the dark.<sup>52</sup> Using a combination of the two polymers,  $\text{PVP-Ru(bpy)}_2\text{Cl}$  on the illuminated electrode and  $\text{PVP-Os(bpy)}_2\text{Cl}$  on the dark electrode (Figure 2), resulted in  $V_{oc} = 1.0 \text{ V}$ .<sup>52</sup> These experiments demonstrated that it was possible to achieve photovoltages as high as  $\sim 1 \text{ V}$  without any equilibrium band bending in a solid-state organic semiconductor film. In other words, the asymmetric dissociation of excitons at an interface *by itself* was capable of producing a powerful photovoltaic effect even when it resulted in an internal electric field that *opposed* further charge separation.

Cells based on another molecular semiconductor, perylene bis(phenethylimide), PPEI (Figure 3), were designed to probe the relative importance of the exciton dissociation process compared to the average internal electric field  $\Phi_{bi}/qd$  ( $d$  = cell thickness).<sup>55</sup> These devices resembled, more closely than our LC porphyrin cells, the typical organic PV cells of the time.<sup>16,17</sup> The organic semiconductor film was much thinner ( $\sim 200 \text{ nm}$ ) than that in the LC porphyrin cells, and the organic layer was sandwiched between two electrodes of different work functions. The internal electric field across the PPEI film was varied by

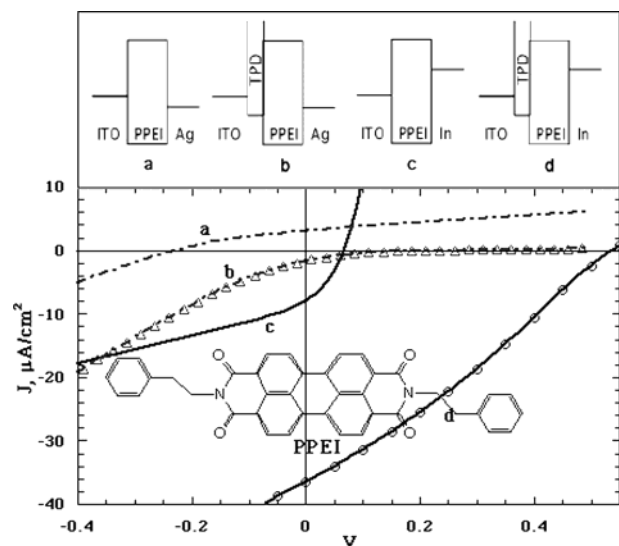


**Figure 3.** Current density–voltage curves for four cells of configuration ITO/X/PPEI (200 nm)/M, where X is either nothing (cells a and c) or a  $\sim 25$  nm thick film of the hole-selective contact, TPD (cells b and d). The metal counter electrode, M, is either Ag or In. The qualitative energy level diagrams of the four types of cells before equilibration are shown. The structure of PPEI is shown. Illumination was  $8 \text{ mW/cm}^2$  at 500 nm. Data from ref 55.

using either Ag or In as back contacts while ITO served as the transparent front contact. The work function of Ag is slightly more positive (further from vacuum) than that of ITO<sup>56</sup> while that of In is more negative.<sup>55</sup> A selective exciton dissociating interface for the PPEI was formed with *N,N'*-diphenyl-*N,N'*-di-(*o*-tolyl)benzidine, TPD, a well-known hole conductor.<sup>57</sup> At the PPEI/TPD interface, excitons in the PPEI can dissociate only via hole injection into the TPD leaving an electron in the PPEI. Cells were constructed in four combinations using either Ag or In as the back contact and with or without a thin film of TPD deposited between the ITO and the PPEI film. Thus, in cells with TPD,  $\phi_{bi}$  would either enhance (with In contacts) or oppose (with Ag contacts) the force generated by interfacial exciton dissociation.

Without the TPD films, the photovoltages were of the polarity expected from the work functions of the electrodes but the photocurrents were quite low (presumably due to inefficient exciton dissociation). The presence of the electroneutral, but hole-selective, TPD films shifted the photovoltage  $\sim 0.45$  V positive in both cases. The application of the TPD film inverted the PV effect in the case of Ag electrodes; that is, the asymmetric dissociation of excitons at the TPD/PPEI interface overwhelmed the influence of the internal electric field. This also demonstrated that the exciton dissociation process was not greatly affected by the field: excitons dissociated efficiently in the polarity opposed to the field. We can conclude that the exciton binding energy was far greater than the internal electric potential drop across the “diameter” of the exciton ( $\sim 1$ – $2$  nm) and that, therefore, exciton dissociation was driven by the band offset at the TPD/PPEI interface (see Figure 4), not by the bulk electric field.<sup>12,38</sup> These experiments demonstrated again that the interfacial dissociation of excitons creates a powerful force affecting the behavior of organic PV cells. This force is sometimes overlooked, although XSCs cannot be properly understood without it. The more or less common assumptions that  $qV_{oc} < \phi_{bi}$  and that exciton dissociation is driven by the electric field at the “p–n junction” are clearly incorrect for XSCs in some, probably most, cases. Recently, results were obtained also in conducting polymer solar cells showing that  $V_{oc}$  is not

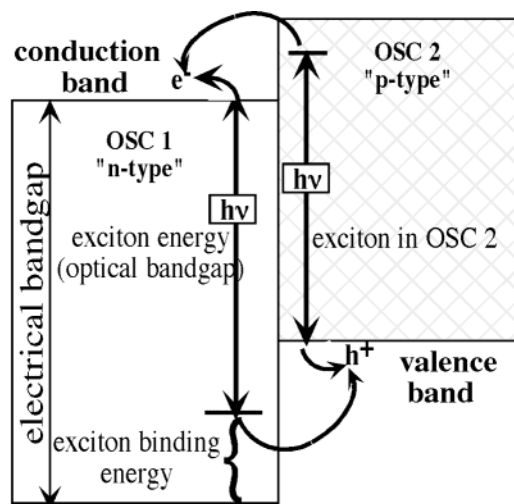


**Figure 4.** Energy level diagram for an excitonic heterojunction solar cell. Excitons created by light absorption in organic semiconductors 1 and 2 do not possess enough energy to dissociate in the bulk (except at trap sites), but the band offset at the interface between OSC 1 and OSC 2 provides an exothermic pathway for dissociation of excitons in both phases, producing electrons in OSC 1 and holes in OSC 2. The band offset must be greater than the exciton binding energy for dissociation to occur.

controlled entirely by  $\phi_{bi}$ , but that the force resulting from interfacial exciton dissociation must be taken into account.<sup>14</sup>

The XSCs discussed so far consisted of only a single organic semiconductor film for simplicity. However, the typical solid-state organic solar cell consists of a bilayer of two organic semiconductors.<sup>16,17</sup> Further studies of PPEI films, now contacted by the photoactive hole-conductor titanyl phthalocyanine, TiOPc,<sup>57</sup> instead of the transparent TPD, showed greatly enhanced photocurrents.<sup>18</sup> These devices were energetically similar to the device shown in Figure 4. Note that such cells are not p–n junctions in any normal sense:<sup>38</sup> they are better described as excitonic heterojunctions. Among other differences, XSCs are majority carrier devices in which the primary processes of carrier generation, separation, and recombination occur at the heterointerface,<sup>12,15,58</sup> while conventional p–n junction solar cells are minority carrier devices in which these processes occur primarily in the bulk of the semiconductors.<sup>38</sup>

The PPEI/TiOPc devices further demonstrated a characteristic common to many (but not all) excitonic solar cells: the dark currents had no quantitative, or even qualitative, relation to the photocurrents.<sup>15,18,58</sup> This is another fundamental distinction between XSCs and conventional solar cells. It occurs primarily because the dark current in XSCs is usually governed by a mechanism different from the photocurrent: the dark current is limited by carrier injection from the electrodes into the photoactive films, while the photocurrent derives from interfacial exciton dissociation. These two processes are distinct and occur at different interfaces. In the typical molecular organic semiconductor with few electroactive impurities (low “dopant” concentration), the dark current can be orders of magnitude lower than the photocurrent under forward bias, and the  $J$ – $V$  curves can have much different shapes in the dark and in the light.<sup>12,18</sup> Nevertheless, a qualitative interpretation of the dark current is still valid: the lower the dark current, the higher the possible photovoltage.<sup>58</sup> In high-surface-area solar cells, there is an additional reason for the lack of quantitative correspondence between the dark currents and photocurrents: There are many possible current pathways through cells made up of interpenetrating bicontinuous phases, and the relative resistance

of these various pathways can change dramatically upon illumination. Thus, dark currents can follow a very different pathway through the device than photocurrents.<sup>15,58</sup> For similar reasons, the cell capacitance (proportional to the *active* surface area) can change by orders of magnitude upon illumination.<sup>59</sup>

#### IV. Exciton Generation, Transport, and Dissociation

In addition to the processes of carrier transport and recombination that are so important in conventional solar cells, exciton transport, recombination, and dissociation are crucial processes in XSCs. In this sense, XSCs are more complicated than conventional solar cells. Some of the characteristics of excitonic solar cells were described in sections II and III; here the focus is on the excitons themselves. The energetic relationships of a typical bilayer XSC are shown in Figure 4.<sup>12</sup> The optical band gap is the energy onset of the optical absorption in the organic semiconductor. This is less than the energy required to produce a free electron and hole (the electrical band gap) because of the low dielectric constant that is typical of organic materials and because of the weak intermolecular electronic interactions (small Bohr radius of carriers).<sup>12</sup> These two effects result in the self-trapping of the incipient charge carrier in the Coulomb field of its conjugate carrier, producing a singlet exciton upon light absorption. We do not treat triplet or charge transfer excitons explicitly, but they are similar to singlets in the context of XSCs. The difference between the electrical and optical band gaps is the singlet exciton binding energy. The thermodynamic requirement for an exciton to dissociate at an interface is that the band offset must be greater than the exciton binding energy (Figure 4). Excitons can also dissociate at electronic trap sites in the bulk leading to one free carrier and one trapped carrier, but this process usually results in photoconductivity rather than in a PV effect (as described earlier in work by Geacintov et al.<sup>45</sup> and by us<sup>13</sup>). However, it should be recognized that this bulk-generation process occurs to a greater or lesser degree in all solid-state XSCs, and it modifies their behavior compared to a “pure” interfacial exciton dissociation mechanism.

The kinetic factors controlling the probability of exciton dissociation at interfaces (or trap sites) are not well understood. It is not known, for example, why organic/organic interfaces are often much more efficient for exciton dissociation than organic/inorganic interfaces.<sup>60</sup> Moreover, there is a tradeoff between rapid exciton motion and efficient quenching. The interfacial electron transfer (quenching) rate must compete with the residence time of the exciton at the interface; thus, rapid exciton transport, while otherwise beneficial, can require ultrafast quenching at the interface for efficient carrier production.<sup>60</sup> There is another factor that affects the interfacial residence time: the exciton energy at the interface can be greater than or less than that in the bulk depending on the lower or higher, respectively, polarizability of the contacting phase.<sup>61</sup> If the polarizability is higher, it tends to trap the exciton near the interface and thus promote dissociation; if the polarizability is lower, the exciton will tend to be reflected from the interface back into the bulk. Interface adhesion (“wetting”), or its absence, can play a role similar to the polarizability.

Measurement of the exciton transport length  $L_{\text{ex}}$  remains an important area of research in XSCs.<sup>60</sup> A seminal paper by Kenkre, Parris, and Schmidt in 1985<sup>62</sup> critically evaluated the  $L_{\text{ex}}$  measurements of the previous few decades and pointed out that most of these studies made a crucial, but unsupported, assumption: they implicitly assumed that the quenching rate of excitons  $S$  within some distance of the quencher was effectively infinite (this was usually expressed as a boundary

condition on the reaction–diffusion equation). Therefore, these studies provided, at best, a lower limit to  $L_{\text{ex}}$ . In fact, Kenkre et al. concluded that most previous measurements had been limited by  $S$ , not by  $L_{\text{ex}}$  as assumed, and thus the actual values of  $L_{\text{ex}}$  were still unknown. Many current studies suffer from the same problem. Only after  $S$  is independently determined to be extremely fast ( $S > 10^5$  cm/s for interfacial quenching) can reliable values for  $L_{\text{ex}}$  be measured. We studied exciton transport in evaporated polycrystalline films of PPEI.<sup>60</sup> Ten different quenching surfaces were investigated. Quenching at oxide semiconductors, such as ITO, SnO<sub>2</sub>, or TiO<sub>2</sub>, was uniformly slow ( $S \sim 10^3$  cm/s); most excitons were reflected from these surfaces. The fastest quencher discovered was poly(3-methylthiophene) where  $S \sim 10^6$  cm/s. Using this quencher, a value of  $L_{\text{ex}} \approx 1.8 \mu\text{m}$  was measured.<sup>60</sup> However, if we had employed only SnO<sub>2</sub>, and assumed that it was an efficient quencher (as has been done before), we would have concluded that  $L_{\text{ex}} \approx 0.07 \mu\text{m}$ . It is clearly important to know if an XSC is limited because most excitons are not reaching the heterointerface (low  $L_{\text{ex}}$ ) or because they are being reflected from the interface without being quenched (low  $S$ ). This information is not available yet for most organic semiconductors. If  $L_{\text{ex}}$  is actually shorter than the optical absorption length  $1/\alpha$ , then the only way all excitons can reach the interface in an optically thick cell is to structure the interface (see below).

Kraebel et al. showed that C<sub>60</sub> is a very fast quencher (<0.2 ps) of excitons in amorphous films of the conducting polymer poly(2-methoxy-5-ethylhexyloxy-phenylene vinylene), MEH-PPV.<sup>63</sup> With this quencher, but unfortunately in a different PPV derivative, Haugeneder et al. measured  $L_{\text{ex}} \approx 14$  nm in the polymer film.<sup>64</sup> The relatively low value of  $L_{\text{ex}}$  in a number of conducting polymers is generally accepted. However, there are still very few unambiguous studies that measure both  $L_{\text{ex}}$  and  $S$  in the same conducting polymer. The  $\sim 100$ -fold difference between the values of  $L_{\text{ex}}$  in PPEI and in PPV derivatives can be rationalized by the highly ordered structure of the PPEI films and by the existence of a high density of intra-band gap (quenching) states in the amorphous PPV film. A clear understanding of the factors that effect  $L_{\text{ex}}$  and (especially)  $S$  in organic semiconductors is still lacking.

The thermodynamic limits to the solar conversion efficiency of a device like that shown in Figure 4 are apparently the same as those of an inorganic heterojunction device:<sup>1</sup> the effective band gap is the difference between the conduction band of the electron conductor (OSC1) and the valence band of the hole conductor (OSC2). However, the efficiency that can be realistically achieved from such a device is not yet known. The most advanced of the current XSCs, the dye-sensitized solar cell, is a very different design from that shown in Figure 4. The DSSC also offers a particularly simple system in which to study some XSC properties because, in it, both exciton transport and internal electric fields are negligible.

#### V. Studies of Dye-Sensitized Solar Cells

The sensitization of wide band gap semiconductors by adsorbed monolayers of dye molecules began in the late 1960s with the work of Gerischer<sup>65</sup> and Memming.<sup>66</sup> A conceptual and practical breakthrough occurred in the late 1980s when Grätzel and co-workers started using high-surface-area semiconductors for dye-sensitized solar cells.<sup>4,5,29,49,67</sup> A sintered film of  $\sim 15$  nm nanocrystalline TiO<sub>2</sub> particles, with an effective surface area  $\sim 1000$  times higher than the geometrical area of the electrode, enabled a monolayer of sensitizing dye to absorb

~99% of the incident sunlight at its absorption maximum. A concentrated redox electrolyte solution that permeated the TiO<sub>2</sub> film allowed the transfer of holes from the oxidized dye to the solution and ultimately to the counter electrode. The use of high-surface-area (nanoporous) substrates was quickly recognized as a major advance in dye-sensitization, but it had consequences beyond just increasing the amount of light a monolayer could absorb, and these were recognized more slowly. For example, effective sensitization of a *planar* semiconductor electrode required band bending in the semiconductor in order to separate the injected electron from its conjugate hole (or “image charge”).<sup>68,69</sup> Without band bending, the Coulomb attraction between the two charge carriers led to rapid recombination. However, the nanosized semiconductor particles used in DSSCs were too small and too lightly doped to support band bending. The key to efficient charge separation in DSSCs was something new: (1) the kinetically ultraslow interfacial recombination rate<sup>4,58</sup> and (2) the ability of electrolyte ions to almost surround each nanoparticle, thus neutralizing the electrostatic field between the photoinjected electron and the hole.<sup>15,59,70</sup>

The concentrated electrolyte solution permeating the nanoporous semiconductor film in a DSSC plays several important roles. The most obvious is that it carries the photoproduced hole to the counter electrode, thus completing the electrical circuit in the cell. Also, as just mentioned, it neutralizes the *nanoscopic* photogenerated electric fields resulting from the dye photoinjection process that would otherwise drive recombination. Finally, the electrolyte also eliminates internal *macroscopic* electric fields in DSSCs, both in the dark and under illumination. Therefore, DSSCs are, in essence, electric-field-free solar cells.<sup>4,15,59,71</sup> (The solid state XSCs discussed in sections II and III were field-free only at equilibrium, but there was no means of neutralizing the photoproduced Coulomb attraction between separated electrons and holes under illumination.) The only locations where an electric field can exist in a DSSC is in the ~1 nm thick electrochemical double layer at the solution/solid interfaces, or at the ~15 nm thick interface between the F-doped SnO<sub>2</sub> substrate and the solution side of the first contacting particle of the TiO<sub>2</sub> film.<sup>15,48,72</sup>

There has been a recent discussion about how DSSCs function. Several groups<sup>72–74</sup> postulated that the PV effect in DSSCs was driven by  $\phi_{bi}$ , as it is in conventional solar cells. The best-defined of these models predicted that the electrical potential difference (junction potential) between the F-SnO<sub>2</sub> substrate and the redox potential of solution, falling across the first contacting particle of the TiO<sub>2</sub> film, set an upper limit to the photovoltage in DSSCs.<sup>72</sup> If true, DSSCs would be subject to the same limitation as conventional solar cells:  $qV_{oc} < \phi_{bi}$ . We refer to this model as the “junction model”. Given our experience with other XSCs, we were skeptical of this model since it neglected the driving force generated by asymmetric interfacial exciton dissociation. We attempted to clarify and make more explicit<sup>48</sup> the common understanding of DSSCs<sup>28,30,31,49,59,71,75</sup> that, in one way or another, accepted interfacial exciton dissociation as a driving force. We ultimately called this the “interface model”.<sup>15</sup> To distinguish between the junction and interface models, we tested the dependence of  $V_{oc}$  on the difference ( $\approx \phi_{bi}$ ) between the work functions of the substrate electrode and the redox solution: the junction model predicted a linear dependence, while the interface model predicted little or no dependence of  $qV_{oc}$  on  $\phi_{bi}$ . The experimental results were unambiguous:  $V_{oc}$  was practically independent of  $\phi_{bi}$  for four different substrates in three different redox solutions (Figure 5).<sup>15,48</sup>

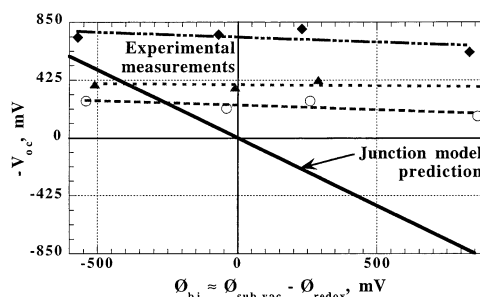


**Figure 5.** The open circuit photovoltage plotted vs the difference between the work function of the substrate in a vacuum  $\phi_{sub,vac}$  and the solution redox potential  $\phi_{redox}$ . The work function of the substrate in the solution  $\phi_{sub}$  is difficult to measure directly but is related to  $\phi_{sub,vac}$ . The four types of substrates are, from left to right, ITO, SnO<sub>2</sub>, Au, and Pt; the filled diamonds are for 0.5 M LiI solution, the open circles are for 0.05 M ferrocene in 0.1 M LiClO<sub>4</sub> solution, and the filled triangles are for 0.05 M hydroquinone in 0.1 M LiClO<sub>4</sub> solution. The theoretical line (solid) shows the behavior predicted by the junction model. (Data from ref 48.)

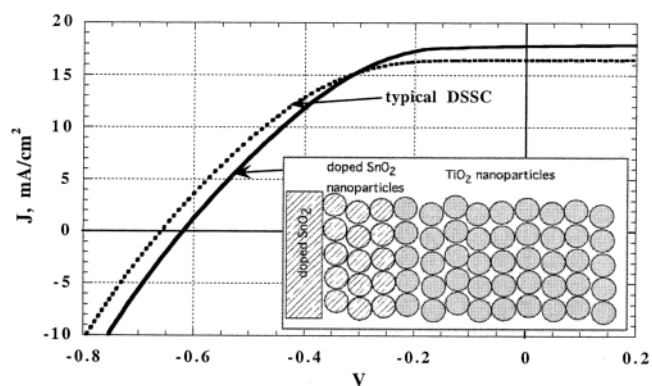


**Figure 6.**  $J$ - $V$  curves of typical DSSCs compared to DSSCs with a 300 nm film of nanoporous doped SnO<sub>2</sub> interposed between the doped SnO<sub>2</sub> substrate and the nanoporous TiO<sub>2</sub> film. Data are the average of two cells of each type. They show that the putative electrical junction at the TiO<sub>2</sub>/doped SnO<sub>2</sub> interface plays no observable role in the photoconversion process of DSSCs.<sup>76</sup>

As mentioned, DSSCs are in some ways the conceptually simplest of the XSCs. Therefore they can provide the most definitive tests of some hypotheses: for example, the hypothesis that  $V_{oc}$  is not controlled by  $\phi_{bi}$ . The results shown in Figure 5 seem unambiguous. However, to further confirm this hypothesis which is of critical importance in understanding XSCs, we moved the putative junction between the doped SnO<sub>2</sub> and the redox solution out into the solution. Here it was surrounded by electrolyte ions that eliminated any influence of an electric field at this “junction”. This was accomplished by interposing a film made from doped nanocrystalline SnO<sub>2</sub> (Alfa) between the substrate and the nanocrystalline TiO<sub>2</sub> film.<sup>76</sup> In this structure (Figure 6), the only possible location for an unscreened junction field, aside from the Helmholtz layers, is between the doped SnO<sub>2</sub> substrate and the doped SnO<sub>2</sub> nanoparticles. In an electrical junction between two such similar materials,  $\phi_{bi}$  is expected to be <100 meV. Nevertheless, under illumination, these cells were practically identical to cells made without the nanocrystalline doped SnO<sub>2</sub> film (Figure 6):  $V_{oc}$  was ~0.65 V and  $J_{sc}$  was ~17 mA/cm<sup>2</sup> in both types of cells. From this and from the previous experiments, we conclude that *internal electric fields play no observable role in DSSCs*. And it is worth noting that, so far, DSSCs are the most efficient of the existing organic-based “alternative” solar cells. Clearly, the conventional model of solar cells fails to accurately describe DSSCs, as it failed for the solid-state organic semiconductor cells described earlier. The con-

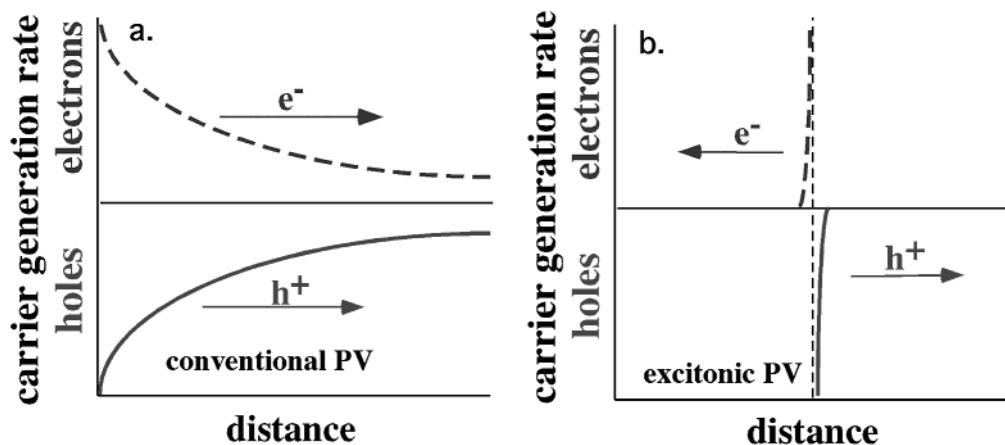


**Figure 7.** An illustration of the fundamental difference in charge carrier-generation mechanisms in conventional (a) and in excitonic (b) solar cells. In conventional solar cells (a), electrons and holes are photogenerated together wherever light is absorbed. Therefore, the photoinduced chemical potential energy gradient  $\nabla\mu_{hv}$  (represented by arrows) drives both carrier types in the same direction (although it has a greater influence on minority carriers). In the excitonic cell (b), electrons are photogenerated in one phase while holes are generated in the other via interfacial exciton dissociation (the phase boundary is denoted by the vertical dashed line). Carrier generation is simultaneous to, and identical with, carrier separation across the interface in XSC cells;  $\nabla\mu_{hv}$  therefore drives electrons and holes in *opposite* directions.

ventional model must overlook some fundamental aspect of XSCs. We suggest that it neglects the driving force created by interfacial exciton dissociation.

Although there are no “substantial” electric fields in DSSCs, this assertion must be defined carefully. As mentioned in section II, in general, if there is no electric field in a solar cell at equilibrium, there must be a photogenerated electric field under illumination that opposes further charge separation. A great virtue of the DSSC is that it confines this photogenerated field to such a small volume at the solid/solution interface (a Debye length of  $\sim 1$  nm) that it presents only an insignificant barrier to carrier transport.<sup>48</sup> This is not the case for nonelectrolyte-containing XSCs.

Although the “exciton” in DSSCs does not have to move anywhere, since it is created directly at the interface, I include DSSCs in the general category of XSCs because they are mechanistically similar to the other XSCs and quite distinct from conventional solar cells. Neither exciton transport nor the presence or absence of internal electric fields is the characteristic that truly distinguishes conventional from excitonic solar cells. Rather, the distinguishing characteristic is the photogeneration of electrons on one side of a heterointerface in XSCs, already separated from the holes photogenerated on the other side.

## VI. Theoretical Description of Conventional and Excitonic Solar Cells

There turns out to be a simple but fundamental distinction between XSCs and conventional solar cells, and it is described in equations here and shown pictorially in Figure 7. Conventional cells, by definition, function according to a photoconversion mechanism which is epitomized by silicon p–n junction solar cells. This mechanism, or its heterojunction analogue, is often applied incorrectly to describe XSCs. Here, in the spirit of nonequilibrium thermodynamics,<sup>77</sup> we review the generalized forces that drive a flux of electrons through a solar cell. We avoid any device-specific assumptions in order to make this treatment valid for all types of solar cells. For simplicity, we treat only a one-dimensional geometry. This can also qualitatively describe the nanostructured cells—DSSCs and bulk heterojunctions—but a quantitative treatment of them would require consideration of all three dimensions.

Gibbs<sup>78</sup> defined the electrochemical potential energy  $E$  as the sum of the electrical and chemical potential energies  $E = U +$

$\mu$ . The spatial gradient of a potential energy is a force; thus,  $\nabla E$  is the fundamental force that drives the charge carrier fluxes through solar cells and other electrical devices (ignoring magnetic fields, temperature or pressure gradients, etc.). The general kinetic expression for the one-dimensional current density of electrons  $J_n(x)$  through a device is

$$J_n(x) = n(x)\mu_n\nabla U(x) + kT\mu_n\nabla n(x) \quad (1)$$

where  $n(x)$  is the concentration of electrons,  $\mu_n$  is the electron mobility (not to be confused with the chemical potential energy  $\mu$ ), and  $k$  and  $T$  are Boltzmann’s constant and the absolute temperature, respectively. An exactly analogous equation describes the flux of holes. Equation 1 is valid both at equilibrium and away from it, both in the dark and in the light.

The quasi (i.e., nonequilibrium) Fermi level for electrons in a semiconductor is defined as

$$E_{Fn}(x) = E_{cb}(x) + kT \ln\{n(x)/N_c\} \quad (2)$$

where  $E_{cb}(x)$  is the electrical potential energy of the conduction band edge,  $E_{cb}(x) = U(x) + \text{constant}$ , and  $N_c$  is the density of electronic states at the bottom of the conduction band. Taking the gradient of eq 2 and substituting it into eq 1 provides the simplest expression for the electron current:

$$J_n(x) = n(x)\mu_n\nabla E_{Fn}(x) \quad (3)$$

Thus, whenever  $\nabla E_{Fn} \neq 0$  ( $\nabla E_{Fp} \neq 0$ ), an electron (hole) current will flow through the device.

Equation 3 shows that the flux of electrons  $J_n$  is related to the (photo)electrochemical force  $\nabla E_{Fn}$  by a proportionality factor,  $n\mu_n$ . Equation 3 and the related equation for holes can be employed as a simple and powerful description of solar cells. They show that *any* photoprocess that generates a nonzero value of  $\nabla E_{Fn}$  and/or  $\nabla E_{Fp}$  will result in a photovoltaic effect. This can be accomplished in several different ways, only one of which is employed in conventional p–n junctions. However, eq 3 does not yet reveal the major difference between the photoconversion mechanisms of conventional and excitonic PV cells. For this, it is necessary to break  $\nabla E_{Fn}$  into its quasi-thermodynamic components  $\nabla U$  and  $\nabla\mu$ . Equation 1 can be separated into two independent electron fluxes, each driven by one of the two forces  $\nabla U$  and  $\nabla\mu$ .

$J_n$  due to the electrical potential energy gradient is

$$J_n(x) = n(x)\mu_n \nabla U(x) \quad (4a)$$

$J_n$  due to the chemical potential energy gradient is

$$J_n(x) = n(x)\mu_n kT/n(x) \nabla n(x)$$

or

$$J_n(x) = n(x)\mu_n \nabla \mu(x) \quad (4b)$$

Again, these equations are equally valid in the light and in the dark. It follows that eq 3 can be expressed as

$$J_n(x) = n(x)\mu_n \{ \nabla U(x) + \nabla \mu(x) \} \quad (5)$$

While  $n(x)$  and  $\mu_n$  influence the magnitude of the electron flux,  $\nabla U(x) + \nabla \mu(x)$  controls its direction. We employ the symbols  $\nabla U_{hv}$  and  $\nabla \mu_{hv}$  to denote the two fundamental forces in a solar cell under illumination.

Equation 5 shows that the electrical potential energy gradient  $\nabla U$  and the chemical potential energy gradient  $\nabla \mu$  are *equivalent* forces. This equivalence is sometimes overlooked because of the predominant importance of  $\nabla U$  in conventional PV cells that results primarily from two factors: (1) the photogeneration of carriers throughout the bulk and (2) their high mobilities that allow them to quickly “equilibrate” their spatial distributions regardless of their point of origin. Both of these factors minimize the influence of  $\nabla \mu_{hv}$ . However, in XSCs, almost all carriers are photogenerated in a narrow region near the interface, leading to a photoinduced carrier concentration gradient (proportional to  $\nabla \mu_{hv}$ ) that is much higher and qualitatively distinct from that in conventional PV cells (Figure 7). This effect, coupled with the spatial separation of the two carrier types across the interface upon photogeneration (Figures 4 and 7b), constitute a powerful photovoltaic driving force. This is further enhanced by the generally low equilibrium charge carrier density making  $\nabla \mu_{hv}$  often the dominant driving force in XSCs. For example,  $\nabla U$  can be  $\sim 0$  in the bulk and a highly efficient solar cell can be made based wholly on  $\nabla \mu_{hv}$ . This is how DSSCs function. In solid-state organic PV cells without mobile electrolyte, both  $\nabla U$  and  $\nabla \mu$  must be taken into account.

$\nabla \mu$  plays a role in the current flow of all electronic devices, but its importance declines as the equilibrium carrier concentration increases. In metals, for example, the carrier concentration is so high that no significant concentration gradients can be achieved; therefore, the second term in eq 1 can be neglected. In highly doped semiconductors, significant values of  $\nabla \mu_{hv}$  are usually achieved only in the minority carrier density. However,  $\nabla \mu_{hv}$  is more important in organic materials where the equilibrium carrier density is very low. Of course,  $\Phi_{bi}$  still plays a role in XSCs. For photoconversion to be efficient,  $\Phi_{bi}$  must either promote current flow in the same direction as  $\nabla \mu_{hv}$ , as it does in most solid state XSCs, or it must be strongly screened, as it is in DSSCs.

In all solar cells at equilibrium,  $\nabla U(x) = -\nabla \mu(x)$  for all  $x$  for both electrons and holes. This follows directly from the law of microscopic reversibility and the thermodynamic requirement that  $\nabla E(x) = \nabla U(x) + \nabla \mu(x) = 0$  at equilibrium. The chemical and electrical potential energy gradients are always counterpoised at equilibrium. In a conventional solar cell, they are both large at equilibrium and *decrease* under illumination, eventually approaching zero as the bands flatten. In many XSCs (e.g., the symmetrical cells described in sections II and III and in DSSCs),

both forces are small at equilibrium and *increase* under illumination—another fundamental difference with conventional cells.

The maximum photovoltage obtainable in any solar cell at a given light intensity  $I$  can be derived from eq 3. Since  $\nabla E_{Fn}$  and  $\nabla E_{Fp}$  are the driving forces for the fluxes of electrons and holes, respectively, net current flow must stop when these gradients either simultaneously become zero (the ideal cell) or when the electron flux exactly cancels the hole flux (nonideal cell). The maximum photovoltage in an ideal PV cell is thus given by the maximum splitting between the quasi Fermi levels anywhere in the cell at open circuit, since an applied potential difference greater than this will cause the photocurrent to reverse its direction.<sup>12</sup>

$$qV_{oc,max}(I) = (E_{Fn} - E_{Fp})_{max} \quad (6)$$

The photovoltage in a real solar cell  $V_{oc}(I)$  is usually less than  $V_{oc,max}(I)$  because of recombination processes, mass transfer limitations, etc. Under the assumption of ohmic contacts, that is, assuming there is no voltage drop across the semiconductor/contact interfaces, the photovoltage in a real cell is

$$qV_{oc}(I) = E_{Fn,x=0} - E_{Fp,x=d} \quad (7)$$

where  $x = 0$  and  $x = d$  correspond to the negative and positive contacts, respectively, of the solar cell.  $V_{oc}$  is usually a logarithmic function of light intensity because of the logarithmic dependence of  $E_{Fn}$  on  $n$ , see eq 2.

In general, the photovoltage of a solar cell is a function of *both* the built-in electrical *and* the photoinduced chemical potential energy differences across the cell. The common assumption that  $\Phi_{bi}$  alone sets the upper limit to the photovoltage (as  $I \rightarrow \infty$ )<sup>17,33,34</sup> is clearly not true. However, it *is* approximately true for a specific photoconversion mechanism—the mechanism governing conventional solar cells: When both electrons and holes are photogenerated together in the same semiconductor phase (Figure 7a), and thus have the same spatial distribution,  $\nabla \mu_{hv}(x)$  drives them both in the same direction (although it may be a small force). To separate electrons from holes then requires the only other available force,  $\nabla U_{hv}$ . Therefore, in this case,  $\Phi_{bi}$  ( $= \int \nabla U dx$  at equilibrium) sets the upper limit to  $qV_{oc}$  *because*  $\Phi_{bi}$  is required for charge separation. (We ignore small effects such as Demer potentials for simplicity.)<sup>13,42</sup>

Excitonic solar cells are fundamentally different. The charge carrier pairs are already separated across an interface upon photogeneration, creating a large  $\nabla \mu_{hv}$  (Figure 7b) which tends to separate them further. An internal electric field is not required for charge separation and thus  $\Phi_{bi}$  does *not* set the upper limit to  $V_{oc}$ . We showed above that substantial PV effects can be achieved in both solid-state organic PV cells and in DSSCs under conditions where  $\Phi_{bi} \approx 0$ . Numerical simulations of DSSCs<sup>79</sup> also have shown that  $V_{oc}$  can be nearly independent of  $\Phi_{bi}$ , while simulations of organic PV cells showed that  $V_{oc}$  is commonly greater than  $\Phi_{bi}$ .<sup>12</sup>

## VII. Simulations of Conventional and Excitonic Solar Cells

There are numerous differences between conventional semiconductors, such as silicon, and organic semiconductors, such as perylene diimides, or conducting polymers. To name just a few, there are major differences in bandwidths, Madelung constants, carrier mobilities, defect densities, dielectric constants, purities, doping levels, etc. All of these factors play an important role in the *quantitative* differences between conventional and

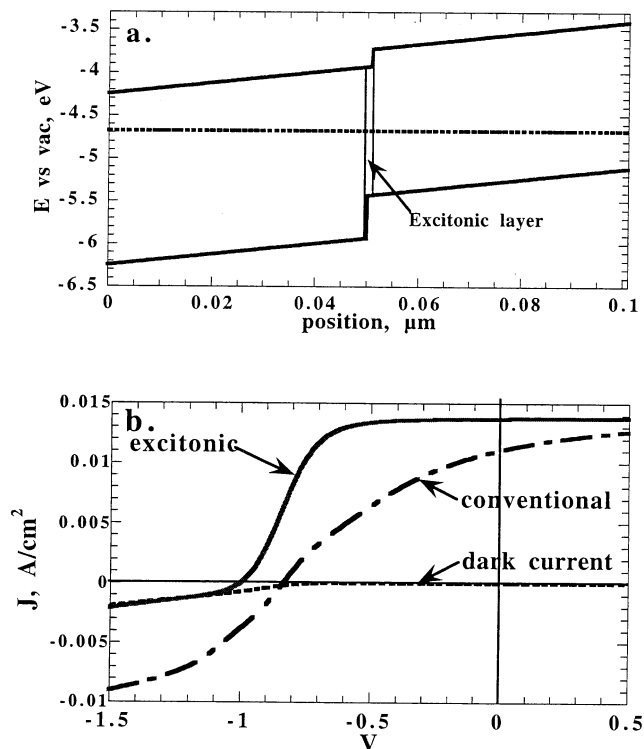


**Figure 8.** (a) Band diagram of the simulated solar cells (conventional and excitonic) at equilibrium. In the conventional cell, the exponential absorption coefficient is  $\alpha = 10^5 \text{ cm}^{-1}$  throughout the cell; in the excitonic cell, light is absorbed only within 1 nm of the interface (the “excitonic layer”) with  $\alpha = 10^7 \text{ cm}^{-1}$ . (b) The calculated  $J$ - $V$  curves under  $50 \text{ mW/cm}^2$  illumination ( $31.6 \text{ mW/cm}^2$  is absorbed) at  $\lambda = 2.1 \text{ eV}$ . The only difference between the conventional and excitonic cells is the spatial distribution of the photogenerated charge carriers. The dark current is identical for both devices.

excitonic solar cells. Yet, it is the theme of this article that there is one unique factor that accounts for the *qualitative* differences between them: the spatial distribution of the photogenerated charge carriers (see Figure 7). To demonstrate the significance of this seemingly small difference, we performed numerical simulations to compare two heterojunction solar cells in which every parameter was identical except the location of the photogenerated charge carriers.

New results from a simulation similar to those reported before<sup>12</sup> are shown in Figure 8. This simulation involves a somewhat more realistic solar cell than treated before. It incorporates band bending ( $\phi_{bi} = 0.64 \text{ V}$ ) resulting from the assumed doping densities of  $n_d = n_a = 10^{12} \text{ cm}^{-3}$  on the left- and right-hand sides, respectively, of the device and ohmic contacts to each side. The band gaps, band offsets, and doping densities are loosely based on a perylene diimide/metallophthalocyanine cell (left- and right-hand sides, respectively).

We employed the freeware simulation program SimWindows (<http://www-ocs.colorado.edu/SimWindows/simwin.html>).<sup>12,80</sup> It numerically solves the coupled differential equations for each carrier type (transport, continuity, and Poisson’s) that describe optoelectronic phenomena in semiconductor devices. By design, it equates light absorption with charge carrier generation. To adapt it to compare conventional to excitonic PV cells, we made the following assumption for the XSCs:<sup>12</sup> light absorption occurs only in a 1 nm thick “excitonic layer” at the heterojunction between the two organic semiconductors (Figure 8a). In other words, we neglect exciton transport and assume that all excitons are created and dissociate in the excitonic layer. We set the conduction band edge of the “excitonic layer” at the potential

of the “*n*-type” semiconductor and the valence band edge at the potential of the “*p*-type” semiconductor.<sup>12</sup> Light absorption in this layer thus naturally leads to electron transfer to the left, and hole transfer to the right (Figure 8a) as well as to recombination in the excitonic layer. This is a reasonable, but not perfect, approximation to the effect of the interfacial dissociation of excitons.<sup>12</sup>

The excitonic layer was also included in the conventional PV device, but in this case, the light absorption coefficient was set constant throughout the cell. When illuminated, the light is incident on the left-hand side. All carrier mobilities are set to  $0.1 \text{ cm}^2/\text{V s}$ . The only difference between the conventional and excitonic PV cells in our comparison is that the absorption coefficient is  $\alpha = 10^5 \text{ cm}^{-1}$  everywhere throughout the 101 nm thick conventional PV cell, while  $\alpha = 10^7 \text{ cm}^{-1}$  in the 1 nm thick “excitonic layer” of the XSC and  $\alpha = 0 \text{ cm}^{-1}$  elsewhere. The amount of light absorbed is thus practically the same in both cells; only its spatial distribution and, therefore, the spatial distribution of photogenerated charge carriers differ between the simulated cells.

The simulation shows that major differences in PV behavior occur in otherwise identical devices that differ *only* in the spatial distribution of photogenerated carriers (Figure 8b). The conventional cell is much less efficient than the XSC. There are at least two reasons for this: (1) recombination throughout the bulk is more efficient than recombination only at the interface (excitonic layer), given the same rate constants for recombination.<sup>12</sup> (2) As depicted in Figure 7, the XSC has the photogenerated force  $\nabla\mu_{hv}$  operating in concert with  $\phi_{bi}$  separating the two carriers and driving them toward their respective electrodes, while in the conventional cell,  $\nabla\mu_{hv}$  opposes  $\phi_{bi}$ . Thus, the conventional cell produces  $V_{oc} = 0.83 \text{ V}$  while the XSC produces  $V_{oc} = 1.00 \text{ V}$ . (Both of these are greater than  $\phi_{bi} = 0.64 \text{ eV}$  because the band offset at the heterojunction also serves to rectify the photocurrent.)<sup>12</sup> The relative short circuit photocurrents ( $11.1 \text{ mA/cm}^2$  versus  $13.7 \text{ mA/cm}^2$ ) and fill factors (34% vs 59%) strongly favor the XSC. Overall, the simulated XSC has a conversion efficiency more than 2.5-fold higher than the conventional cell. Having two driving forces working in concert (XSCs) is naturally better than having the two forces oppose one another (conventional cells), all else being equal. This is not meant to suggest that XSCs are inherently more efficient than conventional solar cells; most of the quantitative differences mentioned earlier still favor conventional cells. Nevertheless, it is clear that there are essential qualitative differences between the two general classes of solar cells, and given further understanding and development, XSCs might eventually displace conventional solar cells by virtue of being cheaper and having comparable efficiencies.

### VIII. Comparing the Three Existing Types of XSCs: Organic PV Cells with Planar Interfaces, Bulk Heterojunction Cells, and DSSCs

Excitonic solar cells often work best when the organic film is quite thin. Several factors contribute to this including the high electrical resistance of most organic semiconductors, their low carrier mobilities, limited exciton transport lengths, and dissociation rates, etc. Also, the equilibrium electric field, if there is one, caused by electrical contacts with different work functions, is naturally higher for thinner films. Dye-sensitized solar cells embody a “thin film” XSC cell taken to its logical extreme: the organic film is just a single monolayer adsorbed to a substrate such as  $\text{TiO}_2$ .<sup>4,5</sup> Grätzel’s key idea was to make the substrate so highly structured that even this ultrathin organic

film would be optically thick. In DSSCs, both the required exciton and charge carrier transport lengths through the organic film are effectively zero, thus eliminating two of the major limitations of organic materials. Of course, other limitations appear in such a device,<sup>15</sup> but at present, the DSSC is still the most efficient XSC (~10%).

With the success of the DSSC, several groups started structuring the interfaces of other types of XSCs leading to marked improvements in some polymer-based solar cells.<sup>2,3,21–23</sup> The highest solar conversion efficiency achieved so far in polymer cells with a structured interface is about 2.5%,<sup>21</sup> while about 0.7% has been achieved with a planar interface (and different polymers).<sup>24,81</sup> So far, little work has been reported on structuring the interface of molecular semiconductor cells, although a similar effect has been achieved with a light trapping device and a 10 nm thick organic bilayer, resulting in an efficiency of 2.4%.<sup>19</sup>

Both DSSCs and bulk heterojunction cells have a highly convoluted internal geometry that promotes exciton dissociation, leading to efficient charge generation and separation. The same physical principles that apply to planar junctions apply also to them, of course. However, it is more difficult to visualize, and to calculate, the forces when the interface is nanostructured in three dimensions. Although charge carrier generation occurs throughout the “bulk” in these cells, it occurs via interfacial exciton dissociation resulting in electrons in one phase and holes in the other. Therefore, the cells behave as XSCs rather than as conventional PV cells.<sup>12</sup> To be efficient, solid-state XSCs without mobile electrolyte, whether nanostructured or not, require a built-in potential to overcome the photogenerated Coulomb field between separated electrons and holes that would otherwise drive recombination.

The only location where substantial recombination can occur in an XSC is at the exciton-dissociating heterointerface, since this is the only location where substantial numbers of electrons and holes coexist. Bulk recombination, the major recombination process in conventional cells, can usually be neglected in XSCs because the bulk density of minority carriers is insignificant.<sup>12</sup> Therefore, all else being equal, the greater the surface area of an XSC, the faster the interfacial recombination rate. That is, there is a tradeoff between enhancing exciton dissociation by increasing interfacial surface area and enhancing recombination. The DSSC lies at one extreme, having the highest surface area of any XSC and thereby requiring the slowest interfacial recombination reactions, compared to the photoinjection and transport processes. The required ultraslow interfacial recombination can be achieved only with a few redox couples, most commonly  $I^-/I_2$ .<sup>58,82,83</sup> The reduction of  $I_2$  is very slow (self-exchange rate of  $\sim 10^2 \text{ M}^{-1} \text{ s}^{-1}$ )<sup>84</sup> on  $TiO_2$  and  $SnO_2$  surfaces<sup>58</sup> unless catalyzed (by Pt, for example). Thus, using the  $I^-/I_2$  couple and applying catalyst only to the counter electrode, while the photovoltaic process occurs on the working electrode, creates the conditions necessary for efficient photoconversion in a DSSC.

Bulk heterojunction cells have a nanostructured morphology similar to DSSCs but are usually ~100-fold thinner (~100 nm versus ~10  $\mu\text{m}$  for a DSSC), since the light absorber is also the hole conductor. They also lack mobile electrolyte and, therefore, electric fields must be taken into account in their description. In the most efficient cells to date, an electron conducting nanoparticulate phase (e.g., derivatized  $C_{60}^{21}$  or CdTe quantum rods<sup>23</sup>) is dispersed at a concentration substantially above its percolation threshold in a hole conducting polymer phase. Excitons generated in either phase dissociate at the

nanostructured interface. Electrical contacts are made from two materials with different work functions, e.g., ITO and Al, and the associated built-in field helps drive electrons to the Al contact and holes to the ITO contact. As in DSSCs, it is primarily by virtue of the large (and still poorly understood) asymmetry between the rapid interfacial exciton dissociation rate and the very slow interfacial recombination rate that a substantial PV effect is achieved.<sup>63</sup> Understanding the factors that control the interfacial recombination rates is an important topic for future studies.<sup>85</sup> Although much remains to be learned about bulk heterojunction cells, it is safe to say that  $\nabla\mu_{hv}$  plays a role in them very similar to its role in DSSCs, but modified by the presence of both bulk and nanoscopic electric fields. Therefore,  $V_{oc}$  in bulk heterojunction cells is a function of both  $\Phi_{bi}$  and  $\nabla\mu_{hv}$ , as well as being strongly dependent on the interfacial recombination rate. Some of the advantages and disadvantages of the two different types of interface structuring—substrate structuring, as in the DSSC, or structuring the organic film, as in the bulk heterojunction—were discussed elsewhere.<sup>38</sup>

## IX. Summary

There are fundamental differences in photoconversion mechanism between conventional inorganic solar cells and the primarily organic-based excitonic solar cells. The distinguishing characteristic of XSCs is that charge carrier generation and separation are simultaneous and occur through exciton dissociation at a heterointerface. Electrons are photogenerated on one side of the interface and holes on the other. This contrasts to the spatially and temporally distinct processes of carrier generation in the bulk and subsequent separation in conventional solar cells. The carrier-generation/separation mechanism in XSCs leads to a powerful chemical potential energy gradient  $\nabla\mu_{hv}$  that drives the PV effect, even in the absence of, or in opposition to, a built-in electrical potential energy difference  $\Phi_{bi}$ . The efficiency-limiting factors in XSCs are therefore distinct from those in conventional cells. While the maximum photovoltage achievable in conventional solar cells is limited to less than  $\Phi_{bi}$ , it is experimentally observed to be often substantially greater than  $\Phi_{bi}$  in well-designed XSCs. Numerical simulations show that when two solar cells differ *only* in the spatial distribution of their photogenerated charge carriers, the excitonic cell is substantially more efficient than the conventional cell. XSCs are majority carrier devices where the primary processes of carrier generation, separation, and recombination occur at the heterointerface, while conventional solar cells are primarily minority carrier devices where these processes occur in the bulk semiconductors. Given further understanding and the synthesis of improved materials, XSCs may ultimately displace the more expensive conventional solar cells.

**Acknowledgment.** I thank my co-workers and collaborators, many of whose names appear on our joint publications, and the U.S. Department of Energy, Office of Science, Division of Basic Energy Sciences, Chemical Sciences Division, for supporting this research.

## References and Notes

- (1) Fahrenbruch, A. L.; Bube, R. H. *Fundamentals of Solar Cells. Photovoltaic Solar Energy Conversion*; Academic Press: New York, 1983.
- (2) Yu, G.; Gao, J.; Hummelen, J. C.; Wudl, F.; Heeger, A. J. *Science* **1995**, *270*.
- (3) Halls, J. J. M.; Walsh, C. A.; Greenham, N. C.; Marseglia, E. A.; Friend, R. H.; Moratti, S. C.; Holmes, A. B. *Nature* **1995**, *376*, 498–500.
- (4) Hagfeldt, A.; Grätzel, M. *Acc. Chem. Res.* **2000**, *33*, 269–277.
- (5) O'Regan, B.; Grätzel, M. *Nature* **1991**, *353*, 737–740.
- (6) Kallman, H.; Pope, M. J. *Chem. Phys.* **1959**, *30*, 585.

- (7) Tollin, G.; Kearns, D. R.; Calvin, M. *J. Chem. Phys.* **1960**, *32*, 1013–1019.
- (8) Fox, D.; Labes, M. M.; Weissberger, A. *Physics and Chemistry of the Organic Solid State*; Interscience: New York, 1963; Vol. 1.
- (9) Gutman, F.; Lyons, L. E. *Organic Semiconductors, Part A*; Krieger: Malabar, 1981.
- (10) Pope, M.; Swenberg, C. E. *Electronic Processes in Organic Crystals*; Clarendon Press: New York, 1982.
- (11) Powell, R. C.; Soos, Z. G. *J. Lumin.* **1975**, *11*, 1–45.
- (12) Gregg, B. A.; Hanna, M. C. *J. Appl. Phys.* **2003**, *93*(6), 3605–3614.
- (13) Gregg, B. A.; Fox, M. A.; Bard, A. J. *J. Phys. Chem.* **1990**, *94*, 1586–1598.
- (14) Ramsdale, C. M.; Barker, J. A.; Arias, A. C.; MacKenzie, J. D.; Friend, R. H.; Greenham, N. C. *J. Appl. Phys.* **2002**, *92*, 4266–4270.
- (15) Gregg, B. A. In *Semiconductor Photochemistry and Photophysics*; Schanze, K. S., Ramamurthy, V., Eds.; Marcel Dekker: New York, 2003; Vol. 10, pp 51–88.
- (16) Tang, C. W. *Appl. Phys. Lett.* **1986**, *48*, 183–185.
- (17) Simon, J.; Andre, J.-J. *Molecular Semiconductors*; Springer-Verlag: Berlin, 1985.
- (18) Gregg, B. A. *Chem. Phys. Lett.* **1996**, *258*, 376–380.
- (19) Peumans, P.; Bulovic, V.; Forrest, S. R. *Appl. Phys. Lett.* **2000**, *76*, 2650–2652.
- (20) Heeger, A. J. *J. Phys. Chem. B* **2001**, *105*, 8475–8491.
- (21) Shaheen, S. E.; Brabec, C. J.; Sariciftci, N. S.; Padinger, F.; Fromherz, T. *Appl. Phys. Lett.* **2001**, *78*, 841–843.
- (22) Granström, M.; Petritsch, K.; Arias, A. C.; Lux, A.; Andersson, M. R.; Friend, R. H. *Nature* **1998**, *395*, 257–260.
- (23) Huynh, W. U.; Dittmer, J. J.; Alivisatos, A. P. *Science* **2002**, *295*, 2425–2427.
- (24) Jenekhe, S. A.; Yi, S. *Appl. Phys. Lett.* **2000**, *77*, 2635–2637.
- (25) Brabec, C. J.; Cravino, A.; Meissner, D.; Sariciftci, N. S.; Fromherz, T.; Rispen, M. T.; Sanchez, L.; Hummelen, J. C. *Adv. Funct. Mater.* **2001**, *11*, 374–380.
- (26) Arango, A. C.; Johnson, L. R.; Bliznyuk, V. N.; Schlesinger, Z.; Carter, S. A.; Hörhold, H.-H. *Adv. Mater.* **2000**, *12*, 1689–1692.
- (27) Malliaras, G. G.; Salem, J. R.; Brock, P. J.; Scott, J. C. *J. Appl. Phys.* **1998**, *84*, 1583–1587.
- (28) Kalyanasundaram, K.; Grätzel, M. *Coord. Chem. Rev.* **1998**, *77*, 347–414.
- (29) Nazeeruddin, M. K.; Kay, A.; Rodicio, I.; Humphry-Baker, R.; Müller, E.; Liska, P.; Vlachopoulos, N.; Grätzel, M. *J. Am. Chem. Soc.* **1993**, *115*, 6382–6390.
- (30) Schlichthörl, G.; Huang, S. Y.; Sprague, J.; Frank, A. J. *J. Phys. Chem. B* **1997**, *101*, 8141–8155.
- (31) Södergren, A.; Hagfeldt, A.; Olsson, J.; Lindquist, S.-E. *J. Phys. Chem.* **1994**, *98*, 5552–5556.
- (32) Nozik, A. J. *Physica E* **2002**, *14*, 115–120.
- (33) Fonash, S. J. *Solar Cell Device Physics*; Academic Press: New York, 1981.
- (34) Miller, R. J. D.; McLendon, G. L.; Nozik, A. J.; Schmickler, W.; Willig, F. *Surface Electron-Transfer Processes*; VCH: New York, 1995.
- (35) Boxer, S. G. *Biochim. Biophys. Acta* **1983**, *726*, 265–292.
- (36) Barber, J.; Andersson, B. *Nature* **1994**, *370*, 31–34.
- (37) Baltscheffsky, M. *Current Research in Photosynthesis*; Kluwer Academic: Dordrecht, 1990; Vol. 1.
- (38) Gregg, B. A. In *Molecules as Components in Electronic Devices*; Lieberman, M., Ed.; American Chemical Society: Washington, DC, 2003; pp 243–257.
- (39) Gregg, B. A.; Cormier, R. A. *J. Am. Chem. Soc.* **2001**, *123*, 7959–7960.
- (40) Lonergan, M. C.; Cheng, C. H.; Langsdorf, B. L.; Zhou, X. *J. Am. Chem. Soc.* **2002**, *124*, 690–701.
- (41) Pfeiffer, M.; Beyer, A.; Plönnigs, B.; Nollau, A.; Fritz, T.; Leo, K.; Schlettwein, D.; Hiller, S.; Wörhle, D. *Sol. Energy Mater. Sol. Cells* **2000**, *63*, 83–99.
- (42) Pope, M.; Swenberg, C. E. *Electronic Processes in Organic Crystals and Polymers*, 2nd ed.; Oxford University Press: New York, 1999.
- (43) Popovic, Z. D.; Hor, A.-M.; Loutfy, R. O. *Chem. Phys.* **1988**, *127*, 451–457.
- (44) Campbell, I. H.; Hagler, T. W.; Smith, D. L.; Ferraris, J. P. *Phys. Rev. Lett.* **1996**, *76*, 1900–1903.
- (45) Geacintov, N.; Pope, M.; Kallman, H. *J. Chem. Phys.* **1966**, *45*, 2639.
- (46) Gregg, B. A.; Fox, M. A.; Bard, A. J. *J. Am. Chem. Soc.* **1989**, *111*, 3024–9.
- (47) Yuan, Y.; Gregg, B. A.; Lawrence, M. F. *J. Mater. Res.* **2000**, *15*, 2494–2498.
- (48) Pichot, F.; Gregg, B. A. *J. Phys. Chem. B* **2000**, *104*, 6–10.
- (49) Cahen, D.; Hodes, G.; Grätzel, M.; Guillemoles, J. F.; Riess, I. *J. Phys. Chem. B* **2000**, *104*, 2053–2059.
- (50) Green, M. A. *Third Generation Photovoltaics: Concepts for High Efficiency at Low Cost*; McConnell, R. D., Kapur, V. K., Ed.; Electrochemical Society: Pennington, NJ, 2001; Vol. 2001-10, pp 3–19.
- (51) Würfel, P. *Sol. Energy Mater. Sol. Cells* **1997**, *46*, 43–52.
- (52) Gregg, B. A.; Kim, Y. I. *J. Phys. Chem.* **1994**, *98*, 2412–2417.
- (53) Calvert, J. M.; Schmehl, R. H.; Sullivan, B. P.; Facci, J. S.; Meyer, T. J.; Murray, R. W. *Inorg. Chem.* **1983**, *22*, 2151–2162.
- (54) Gregg, B. A.; Heller, A. *J. Phys. Chem.* **1991**, *95*, 5970–5975.
- (55) Gregg, B. A. *Appl. Phys. Lett.* **1995**, *67*, 1271–1273.
- (56) Grovenor, C. R. M. *Microelectronic Materials*; IOP Publishing: Bristol, 1989.
- (57) Law, K.-Y. *Chem. Rev.* **1993**, *93*, 449–486.
- (58) Gregg, B. A.; Pichot, F.; Ferrere, S.; Fields, C. L. *J. Phys. Chem. B* **2001**, *105*, 1422–1429.
- (59) Zaban, A.; Meier, A.; Gregg, B. A. *J. Phys. Chem. B* **1997**, *101*, 7985–7990.
- (60) Gregg, B. A.; Sprague, J.; Peterson, M. *J. Phys. Chem. B* **1997**, *101*, 5362–5369.
- (61) Zakhidov, A. A.; Yoshino, K. *Synth. Met.* **1994**, *64*, 155–165.
- (62) Kenkre, V. M.; Parris, P. E.; Schmidt, D. *Phys. Rev. B* **1985**, *32*, 4946–4955.
- (63) Kraabel, B.; McBranch, D.; Sariciftci, N. S.; Moses, D.; Heeger, A. J. *Phys. Rev. B* **1994**, *50*, 18543–18552.
- (64) Haugeneder, A.; Neges, M.; Kallinger, C.; Spirkl, W.; Lemmer, U.; Feldman, J.; Scherf, U.; Harth, E.; Gügel, A.; Müllen, K. *Phys. Rev. B* **1999**, *59*, 15346–15351.
- (65) Gerischer, H. *Photochem. Photobiol.* **1972**, *16*, 243–260.
- (66) Memming, R. *Photochem. Photobiol.* **1972**, *16*, 325–333.
- (67) O'Regan, B.; Moser, J.; Anderson, M.; Grätzel, M. *J. Phys. Chem.* **1990**, *94*, 8720–8726.
- (68) Spittler, M. T. *J. Electroanal. Chem.* **1987**, *228*, 69–76.
- (69) Parkinson, B. A.; Spittler, M. T. *Electrochim. Acta* **1992**, *37*, 943–948.
- (70) Gregg, B. A.; Zaban, A.; Ferrere, S. *Z. Phys. Chem.* **1999**, *212*, 11–22.
- (71) Zaban, A.; Ferrere, S.; Gregg, B. A. *J. Phys. Chem. B* **1998**, *102*, 452–460.
- (72) Schwarzburg, K.; Willig, F. *J. Phys. Chem. B* **1999**, *103*, 5743–5746.
- (73) Ditttrich, T.; Beer, P.; Koch, F.; Weidmann, J.; Lauer mann, I. *Appl. Phys. Lett.* **1998**, *73*, 1901–1903.
- (74) Turrion, M.; Macht, B.; Tributsch, H.; Salavatore, P. *J. Phys. Chem. B* **2001**, *105*, 9732–9738.
- (75) Franco, G.; Gehring, J.; Peter, L. M.; Ponomarev, E. A.; Uhlendorf, I. *J. Phys. Chem. B* **1999**, *103*, 692–698.
- (76) We thank Dr. Si-Guang Chen for assistance with these experiments.
- (77) Prigogine, I. *Thermodynamics of Irreversible Processes*; 3rd ed.; Wiley: New York, 1967.
- (78) Gibbs, J. W. *The Scientific Papers of J. Willard Gibbs*; Dover: New York, 1961; Vol. 1.
- (79) Ferber, J.; Luther, J. *J. Phys. Chem. B* **2001**, *105*, 4895–4903. Although the authors did not emphasize this result, see their Figures 9 and 10.
- (80) Winston, D. W. *Physical Simulation of Optoelectronic Semiconductor Devices*; University of Colorado, Boulder, 1996.
- (81) Breeze, A. J.; Salomon, A.; Ginley, D. S.; Gregg, B. A.; Tillmann, H.; Hörhold, H.-H. *Appl. Phys. Lett.* **2002**, *81*, 3085–3087.
- (82) Oskam, G.; Bergeron, B. V.; Meyer, G. J.; Searson, P. C. *J. Phys. Chem. B* **2001**, *105*, 6867–6873.
- (83) Nusbaumer, H.; Moser, J.-E.; Zakeeruddin, S. M.; Nazeeruddin, M. K.; Grätzel, M. *J. Phys. Chem. B* **2001**, *105*, 10461–10464.
- (84) Sun, J.; Stanbury, D. M. *Inorg. Chem.* **1998**, *37*, 1257–1263.
- (85) Wang, Y.; Suna, A. *J. Phys. Chem. B* **1997**, *101*, 5627–5638.